Original article

Textile Research Journal

Textile Research Journal
2015, Vol. 85(1) 80–90

DOI: 10.1177/0040517514538693
trj.sagepub.com

SAGE

Monitoring moisture distribution in textile materials using grating interferometry and ptychographic X-ray imaging

Morteza Esmaeili[1], Jostein B Fløystad[1], Alexander Hipp[2], Marian Willner[2], Martin Bech[2], Ana Diaz[3], Arne Røyset[4], Jens W Andreasen[5], Franz Pfeiffer[2] and Dag W Breiby[1]

Abstract

Employing two recently developed X-ray imaging techniques, we investigated methods for observing moisture at different length scales in organic fibers and textiles. Using the coherent diffractive imaging technique of ptychographic tomography, structural features in a single coated wool fiber in both dry and humid conditions were observed at about 200 nm resolution. The reconstructed three-dimensional images yield quantitative information about the spatial density distribution in the fiber, showing that the fiber swells laterally by 8–9% in humid conditions. We further explore the applicability of grating interferometry, also known as Talbot imaging, for studying humidity transport in woven cotton, with a resolution on the order of 100 μm and a field of view of a few square centimeters. Grating interferometry inherently gives access to three complementary imaging modalities, namely absorption-, phase- and dark-field contrast, and we demonstrate that all of them are valuable and provide complementary information for the purpose of monitoring moisture in textiles.

Keywords

ptychography, talbot imaging, coherent scattering, tomography, textiles, wool, cotton

Due to the increasing demand for clothing systems with improved comfort, function, and safety and the need of the healthcare sector for new biomedical textiles,[1] there are extensive efforts in industry and academia to better understand the characteristics of commonly used fibers and fabrics. Natural textile fibers are important both in traditional garments and in new high-performance clothing systems with customized properties.[2,3] A challenge of scientific and commercial importance is to understand the effects of moisture absorption and desorption on the physico-chemical properties of organic materials in general. Finding ways of monitoring these changes in situ at the macro-, micro-, and nanoscale is desirable. It is commonly known that many natural fibers are strongly affected by humidity and that they are able to absorb substantial amounts of water vapor by swelling.[4] Dimensions, weight, tensile strength, elastic recovery after stretching, and rigidity are amongst the physical properties of fibers that are affected by hydration.[4–6]

Wool is a natural protein fiber which is widely used in textiles, and it has recently received considerable

[1]Department of Physics, Norwegian University of Science and Technology, Norway
[2]Department of Physics, Technische Universität München, Germany
[3]Paul Scherrer Institut, Villigen, Switzerland
[4]SINTEF Materials and Chemistry, Trondheim, Norway
[5]Imaging and Structural Analysis Program, Department of Energy Conversion and Storage, Technical University of Denmark, Denmark

Morteza Esmaeili and Jostein B Fløystad contributed equally to this work

Corresponding author:
Dag W Breiby, Department of Physics, Norwegian University of Science and Technology, Høgskoleringen 5, 7491 Trondheim, Norway.
Email: dag.breiby@ntnu.no

attention for new applications in biomedical and biotechnological products, including tissue engineering, medical implant devices, and bioactive surfaces.[7] A typical wool fiber has an elliptical cross-section with a diameter in the range of 8–70 μm and a length of roughly 5 to 50 cm. It is composed of light elements like carbon, hydrogen, oxygen, nitrogen, and sulfur, and has a highly complicated hierarchical structure.[8] It mainly consists of the *cortex*, which is primarily composed of α-keratins, i.e. protein molecules in α-helix conformation, comprising about 90% of the fiber.[8] This molecular structure gives wool a natural macroscopic crimp, which increases its elasticity and springiness, and also improves the isolating properties of wool by keeping the fibers apart. From a macromolecular point of view, wool is a fibril-reinforced matrix material in which both fibrils and matrix consist of polypeptides. Wool fibers have an outer layer of overlapping scales or *cuticle* responsible for their felting, shrinkage, and insulating properties. Moreover, the scales inhibit accumulation of moisture on the fiber surface, forcing the moisture to reside in the fiber interior, thus making wool feel dry even while holding a considerable amount of water.

Cotton is another classical textile material extensively used in the textile industry, based on its lightweight properties, biodegradable and renewable nature, and high water absorption potential, with a moisture regain of 7–8%.[9] Cotton is a soft, fluffy natural fiber composed mainly of α-cellulose (88–96%) – nature's most abundant natural polymer.[10] The chemical composition of cotton fibers varies slightly, dependent on many variables such as the cultivating environment. It is a well-known fact that cotton is stronger wet than dry, explained by the formation of additional hydrogen bonds between the cellulose molecules. Cotton fibers have so-called convolutions, i.e. natural twists along the entire length of the fiber, that interlock the fibers when spun into yarn. Depending on the location of production of these fibers, the typical length and diameter vary between 1.5–5 cm and 16–20 μm, respectively.[9]

To characterize fibers and textile materials, a variety of techniques[4] including Fourier transform infrared spectroscopy (FTIR), nuclear magnetic resonance (NMR), electron microscopy (SEM, TEM), and X-ray scattering-based methods have been employed. Environmental, or 'wet', SEM is increasingly used, but is essentially a surface-sensitive technique, as it requires sample sectioning to investigate the interior of materials.[11] Because of the non-destructive and penetrating nature of X-rays, X-ray diffraction and imaging are powerful tools to study the structural properties of materials, including at in situ conditions. X-ray fiber diffraction probes the atomic and molecular structures of fibres,[12] but is mainly sensitive to regions with crystalline order, and the results obtained are usually structural averages over the fiber cross-section.

In this study, the novel X-ray methods of ptychography and grating interferometry-based imaging have been employed for monitoring structural effects and transport of humidity in situ in weakly scattering organic fibrous materials. Specifically, we demonstrate the possibility of extracting information about humidity in natural fibers and textiles at two complementary length scales. First, an in situ ptychographic tomography experiment on a single wool fiber under different humidity conditions is discussed. Second, a study on the applicability of imaging by grating interferometry for studying the water uptake and drying process in a cotton fabric in a controlled atmosphere is presented. This article is the first report of X-ray ptychography and grating interferometry applied to wool and cotton samples, representing a step toward the use of these modern X-ray techniques in the textile industry.

Recent X-ray imaging methods

During the last decade pivotal progress has taken place in applied X-ray science. Coherence properties of the X-ray beams have been substantially improved at synchrotrons while advances in X-ray optics have had an impact also in home laboratories, facilitating the development of new X-ray imaging techniques.[13–15] The index of refraction for X-rays is conventionally stated as $n = 1 - \delta + i\beta$. The real part of the refractive index, δ, accounts for refraction, and thus *phase contrast* and can be estimated from the electron density, ρ_e, which is readily available from the material's stoichiometric composition and mass density. The imaginary part β describes absorption, which is approximately proportional to the atomic number to the fourth power Z^4, being the physical explanation for the widespread use of *absorption contrast* radiography in medicine and materials science.

At photon energies above 6 keV imaging techniques based on phase contrast are more sensitive to density variations in the sample and can reveal structures that remain indiscernible in absorption contrast images. This sensitivity increase is related to the fact that for these photon energies, $\delta \sim 10^{-5}$ is at least one order of magnitude higher than its imaginary counterpart $\beta \sim 10^{-7}$. X-ray detectors are insensitive to the phase of the X-ray photons. Phase-contrast measurements thus rely on causing the refracted beam to interfere with a reference beam, giving detectable interference patterns, by placing the detector a suitable distance behind the sample to exploit propagation effects,[16] or by applying phase retrieval techniques to diffraction data.[17] A third contrast mechanism for X-ray imaging

is to base the analysis on the local scattering power of the specimen: more strongly scattering areas will appear brighter, and vice versa.[18] This imaging mode is commonly termed X-ray *dark-field*, and is analogous to dark-field microscopy using visible light.

Ptychography is a version of coherent diffractive imaging (CDI) which circumvents the use of lenses and works with phase retrieval algorithms on recorded Fraunhofer scattering patterns (cf. Figure 1).[19–24] The sample is raster scanned through a micrometer-sized coherent X-ray beam ensuring appropriate overlap between the illuminated areas of neighboring exposures.[20,21] At each position of the raster scan, a far-field coherent X-ray scattering pattern is recorded at ultra-small scattering angles. The scattering patterns are fed into an iterative computer algorithm, yielding reconstructed two-dimensional (2D) phase and amplitude images of the sample.[22,24] In favorable cases of dedicated inorganic test structures, a 2D resolution <10 nm has been demonstrated.[25,26] Rotating the sample and acquiring a sequence of 2D images at different rotation angles provides data that allows three-dimensional (3D) images to be obtained through computed tomography methods.[6,27,28] In synchrotron X-ray tomography, the spatial resolution before the introduction of lens-less imaging techniques was typically 100 nm for hard X-rays and ~50 nm for soft X-rays, often limited by the problems of producing high-quality X-ray lenses.[29] Recently a spatial resolution better than 18 nm has been reported with X-ray ptychographic tomography in 3D for an inorganic test sample.[30] Ptychographic tomography yields quantitative information about the electron density variations in the sample.[28]

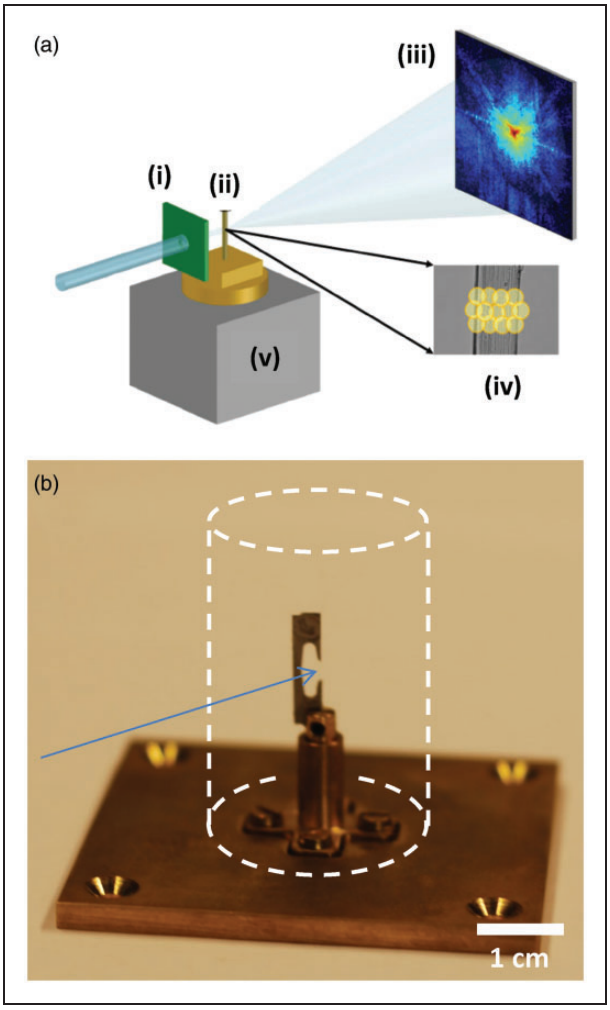

Figure 1. (a) Schematic drawing of experimental setup employed for acquisition of ptychographic tomography data (not to scale). (i) Pinhole for defining the incoming highly coherent X-ray beam, (ii) sample position, (iii) area detector located in the far-field, (iv) illustration of non-periodic raster scanning across a fiber sample, and (v) motors for positioning and scanning the sample. (b) Photograph of the sample holder, with the incoming beam indicated by the arrow. The outlined cylinder gives the approximate dimensions of the sample cap used for humidity control.

Grating interferometric imaging, also known as Talbot imaging, has been attracting much attention for several reasons. It is a Moiré approach, relying on a set of finely pitched gratings to measure the minute angular deflections of refracted beams.[31–34] Because grating interferometry is rather tolerant to low coherence in the incoming beam, a particularly interesting aspect of this technique is that it can be used with traditional X-ray sources, allowing the instrument to be made quite compact.[35] It is expected that the technique will find widespread applications in fields ranging from security screening, via materials and biological science, to medicine.

While the instrumental setup of a grating interferometer, shown in Figure 2, is deceivingly simple, the theory behind it is rather complicated, and only a short outline of the functioning principle will be given here, referring the reader to the rapidly growing literature in this field for an in-depth discussion.[32,34,36] In the case of working with laboratory sources, an additional absorption grating G0 effectively acts as an array of line sources, ensuring a sufficient transverse coherence length for the technique to work.[35,36] In the Fresnel zone after a periodic phase grating (a grating that has negligible absorption but introduces a phase shift) G1 with period g_1, phase modulations are imprinted onto the incoming wave-field. Interference gives rise to repeating intensity patterns known as *Talbot carpets* downstream of the grating.[37,38] At the so-called fractional Talbot distances the contrast of the interference pattern has its maxima. Placing a sample in the incoming wave field will attenuate, refract, and scatter the

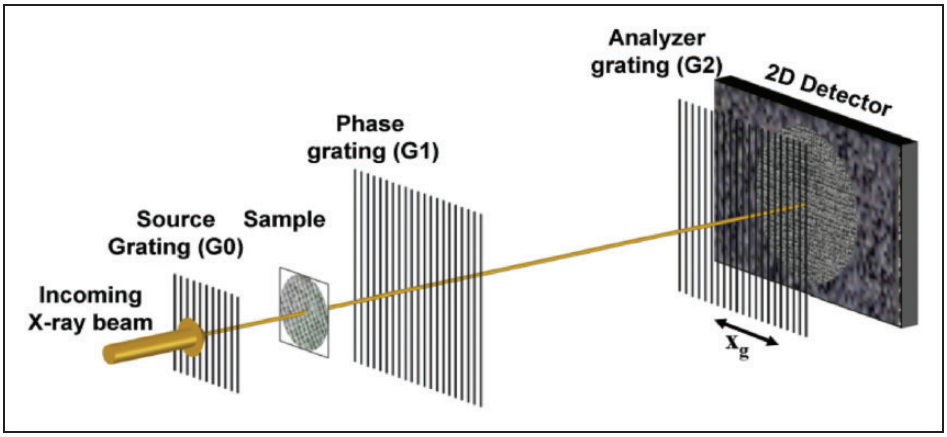

Figure 2. Schematic drawing of Talbot X-ray grating interferometer (not to scale). The sketch shows the source grating G0 acting as a slit array of coherent line sources, a phase grating G1 and an analyzer grating G2. An intensity modulation is detected in the detector pixels when G2 is scanned transversally with respect to G1.

waves, thus perturbing the interference pattern. The Talbot effect can be exploited for imaging by scanning transversely across the repeated intensity pattern using an absorption grating G2 of the same period g_2 as the intensity pattern, known as the "analyzer" grating.[32,34] A sideways translation x_g of G2 will give rise to intensity modulations that are observed in each pixel of the detector placed immediately behind G2. The intensity variation in a given pixel as function of x_g is to a good approximation given by a single Fourier component[31]

$$I(x_g) = a_0 + a_1 \sin\left(\frac{2\pi x_g}{g_2} + \varphi\right) \quad (1)$$

Often the detector pixel size is at least one order of magnitude bigger than the grating period g_2, implying that the signal detected in each pixel will be the average for a large number of grating openings. With a sample in place, *absorption* will reduce the average signal intensity a_0, *refraction* will cause the modulated signal to be shifted laterally as quantified by φ, and small-angle scattering will tend to wash out the modulations, thus decreasing the amplitude a_1. With typical design parameters for a grating interferometer, the images will be most sensitive to features a few micrometer in size.[31,33] Grating interferometry only measures the differential phase contrast along the direction normal to the grating lines, hence it is more sensitive to variations in the refractive index of the sample across than along grating lines.[39]

In summary, combining exposures obtained for different $x_g \in [0, g_2)$, Talbot grating-based imaging yields access to three different imaging modalities based on absorption, differential phase, and dark-field visibility. Complementarily, ptychography is mainly a high-resolution microscopy technique which retrieves the amplitude and phase of both the sample and the incoming wave field. It is timely to ask what the equivalent of the dark-field signal observed in Talbot imaging would be in the case of ptychography. The answer is that the ultra-small-angle scattering in the ptychography case can be considered 'fully exploited' by the large numerical aperture of the technique to provide a high-resolution microscopy image, whereas in the Talbot case of much lower resolution, the signal carrying information about the smaller features in the sample is collected in the 'dark field' signal.

Experimental details

Samples

The ptychography measurements were performed on an isolated chemically coated ('superwashed') merino wool fiber. For the tomography measurements, the approximately 8 mm long fiber was clamped in both ends, carefully keeping it straight without causing elongation.

For the Talbot studies, a piece of thin plain-weaved cotton fabric was investigated. The cotton fiber had been combed, dyed and sanforized prior to weaving. The dimension of the textile piece was approximately $25 \times 25\,\text{mm}^2$, and the grammage was $80\,\text{g/m}^2$.

Ptychography

The ptychographic tomography experiment was carried out at the coherent Small-Angle X-ray Scattering

(X12SA) beamline at the Swiss Light Source, Villigen, Switzerland, using 6.2 keV radiation corresponding to an X-ray wavelength of 2.00 Å. The beam size on the sample was defined by a 2.5 μm pinhole, located 4.5 mm upstream of the sample position. To control the humidity, the sample cell used was as described in detail by Esmaeili et al.[6] The experiment was performed at two extreme humidity conditions, *humid* (cell flushed with humidified N_2, relative humidity >95%) and *dry* (cell flushed with dry N_2, relative humidity <5%). For each projection angle in the tomography experiment, the sample was raster scanned perpendicularly to the incoming beam and illuminated at 408 non-periodically arranged partially overlapping exposures, covering a rectangular field of view of 42 μm (horizontal) × 20 μm (vertical). The scattering patterns were collected using a Pilatus 2 M[40] detector located 7198 mm downstream of the sample position. With an exposure time of 0.2 s, it took approximately 4 hours to perform a full tomography scan, consisting of 176 projections, with a missing wedge of about 5°. The data from 192 × 192 pixels centered around the direct beam was used as input for the ptychography reconstruction algorithm.[22] Based on the 2D reconstructed images obtained for each projection angle, tomographic reconstruction was done using a modified filtered back projection algorithm, after appropriate post-processing steps, as described elsewhere.[41]

Talbot imaging

The Talbot experiment was performed at TU Munich using a grating interferometer operating at the sixth fractional Talbot distance, as previously described in detail.[31,42] A rotating tungsten anode operated at an acceleration voltage of 35 kV and an anode current of 70 mA was used as the X-ray source. The setup was symmetrical with a period of 5.4 μm for G0, G1 and G2. A Dectris Pilatus 100 K detector with pixel size of 172 × 172 μm^2 placed immediately behind G2 was used for recording the signal.[40] The field of view in this experiment was limited by the vertical size of the detector, ~34 mm, corresponding to ~18 mm at the sample position owing to the geometrical magnification in the imaging system. To create stable humidity conditions around the sample, a custom-made sample cell with humidity and temperature sensors was designed. The sample cell was made from aluminum to keep down the weight of the cell, and thin kapton sheets served as windows for the X-ray beams, giving minimal disturbance to the beam wave-front. Acquiring a single reconstructed image took about 45 seconds, consisting of 9 frames at different lateral positions of G2 x_g, each of 5 seconds exposure time. The whole drying experiment reported took 42 minutes.

Results and discussion

Ptychographic tomography applied to a wool fiber

For the ptychography experiment reported here, single wool fibers have been investigated at dry and humid conditions (approximately 5% and 95% relative humidity, respectively) in order to study the effects of water vapor on the morphology of wool. Figure 3(a) shows a representative ptychography projection. In the projection image, faint structures that we assign to the scale surface structures of wool, the *cuticle*, can just be discerned. Figure 3(b) indicates that the fiber interior is essentially dense; however with a couple of pores revealed by their lower electron density. The resolution of the tomograms was better than 200 nm, as determined from the sharpness of the edge of the wool fiber.

For visualizing the measured lateral expansion of the wool, isocontours for $\rho_e = 0.31\ e^-/Å^3$, at both dry and humid states, are also presented (Figure 3(c)), demonstrating that the presence of water in the surrounding atmosphere in the sample cell affects the fiber dimensions. No indications of a longitudinal expansion or contraction were found. Our results thus show an anisotropic, lateral only, swelling of the fiber by approximately 8–9% along each half-axis. In previous studies on the swelling behavior of wool fibers it has been found that water is absorbed by the protein matrix of the fiber which contains hydrophilic groups.[41,43] Note from Figure 3(c) that the pores have shifted radially as the fiber swells, but also tangentially – a fact we speculate might be related to the helical structure of the fibrils in the fiber.

Histograms of the electron densities are shown in Figure 3(d) and exhibit two peaks at $\rho_e = 0$ and $\rho_e = 0.41\ e^-/Å^3$, corresponding to the electron densities of the surrounding atmosphere and the wool fiber, respectively. The negative values arise from noise. Care was taken to ensure that the analysis is based on the very same region of the fiber both in the dry and humid conditions. Knowing the approximate chemical composition of the protein-rich fiber, the mass density of the fiber is estimated to be $\rho_m = (1.25 \pm 0.05)\ g/cm^3$, which compares well to the value 1.29 g/cm^3 reported with other techniques for wool fibers at relative humidity of 95%.[8] Clearly, in the humid state, the number of voxels in the high-electron density peak at 0.4 Å^{-3} has grown at the expense of the low-electron density peak. By careful inspection, it can also be seen in Figure 3(d) that the high-density peak in the histogram has shifted slightly towards the density of water. Integrating the area below the histogram peaks (equivalent to counting the number of voxels containing a high electron density) shows a 17 ± 2% volume increase in the humid state, in full agreement with the observed lateral expansion. These values for volume and radial expansions are

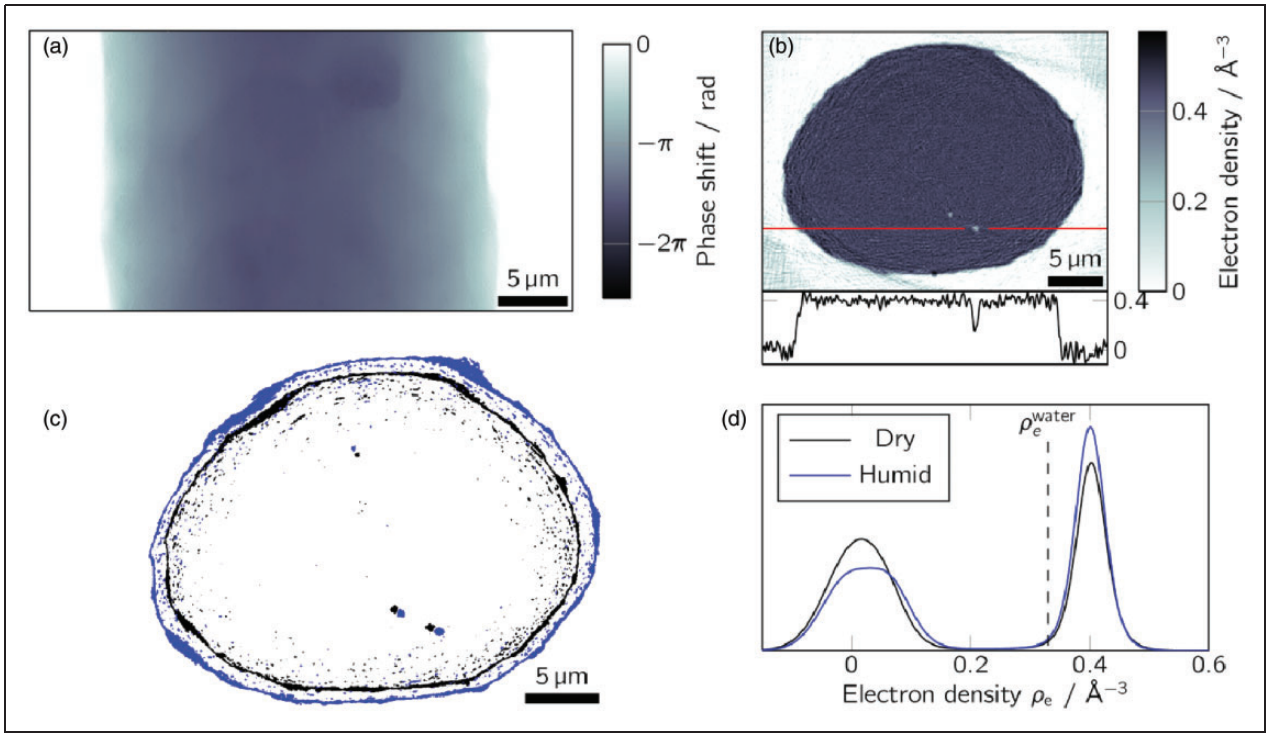

Figure 3. Ptychography results for a wool fiber. (a) A 2D projection phase image (dry state). The scales on the fiber exterior can be discerned as weak lines across the fiber. (b) Tomographically reconstructed cross section of the wool fiber in the dry state, showing an essentially dense material at the current resolution, however with a few less dense pores, as also evident in the extracted line. (c) Isocontours at $\rho_e = 0.31\ e^-/Å^3$ viewed along the fiber axis, demonstrating that the fiber swells uniformly in the plane normal to the fiber main axis. Note the shifts of the pores resolved in the fiber interior. The semi-axes of the fiber cross-section have expanded by 8–9% in the humid state. (d) Histogram of voxel electron density values; see main text for details.

in excellent agreement with results obtained by other methods.[8]

In summary, we have demonstrated that ptychographic tomography is well suited for obtaining three-dimensional images of hydrated organic fibers. In the next section, we shall discuss a complementary technique, also based on coherent X-ray scattering, that can resolve the moisture distribution in macroscopic samples with a resolution of a few hundred microns, opening for systematic studies of diffusion in multi-layered textile samples.

Imaging of moisture distribution in a cotton fabric using grating interferometry

To investigate whether imaging by grating interferometry is suitable for monitoring wetting of textiles, typically by perspiration or water, we have studied a thin cloth of plain-weaved cotton. The experiment was performed by wetting the textile piece with water when it was mounted in the cell, and immediately afterwards starting repeated measurements to monitor the drying process.

Images of the sample before and after drying are shown in Figure 4. In both cases, three images are presented showing the amplitude, differential phase, and dark-field signals. One can see the yarns in the fabrics and some influence of water, while the resolution is insufficient to image the interior of individual yarns of the sample. There are differences between the signals in the dry and wet states of the sample in all three different imaging modalities. Images based on the absorption signal taken in the wet state are blurred by the presence of water in the textile, as water and cotton have rather similar absorption coefficients. In the differential phase-contrast images, the individual yarns of the sample are actually best distinguished in the wet state, emphasizing the complementarity with the absorption signal and suggesting that the differential phase signal is better suited for studying textile samples in wet or humid situations. As expected, the horizontal differential phase-contrast obtained using the vertical gratings is more sensitive to vertical than horizontal yarns.

Whereas the dark-field signal from the wet sample is quite featureless, the dark-field image from the dry sample shows a plethora of details, implying that this signal is highly suitable for monitoring wetting of the textile. Dark-field imaging is the best-suited technique among the three different imaging modes when it comes

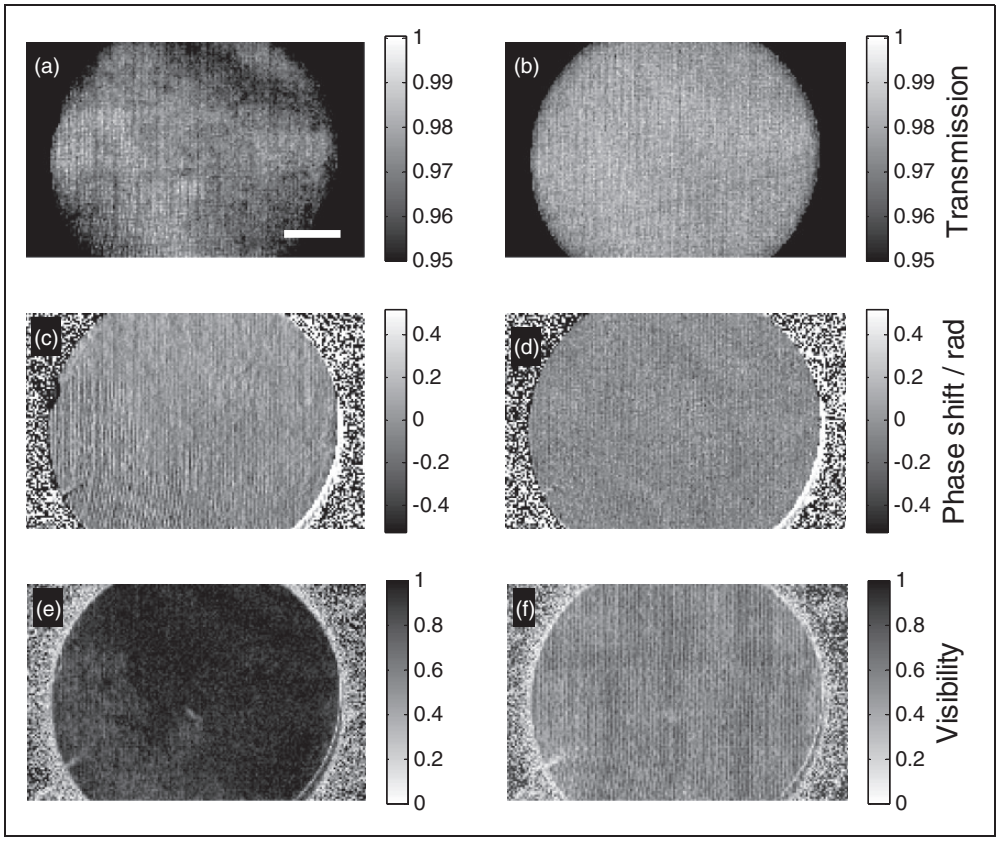

Figure 4. Reconstructed Talbot X-ray grating interferometry images based on (a, b) absorption contrast, (c, d) differential phase-contrast, and (e, f) dark-field images of the cotton fabric piece taken when the sample was soaked with water (left column) and after the sample had completely dried up (right column). For the absorption images the scale bar gives the transmission, which is close to 100% for the textile, and practically 0 % for the sample holder. The phase change associated with propagating through the textile is of the order of $\pi/10$ radians. In the dark-field images, black corresponds to 100% visibility and white to 0% visibility. The field of view is $29.1 \times 18.5\,\text{mm}^2$; the scale bar is 5 mm.

to resolving the texture of the dry cotton fabric (cf. Figure 4(f)). In the dark-field image of the dry sample, detailed information about the size and position of the individual yarns, their sizes, and points of overlapping warp and woof can be retrieved. The contrast disappears in the wet case due to the presence of water reducing the scattering contrast, as the electron density of water is much closer to that of cotton than to air.

To make the resolving power of the different signals more apparent, consider the Fourier transforms of the amplitude, differential phase, and dark-field signals from the sample in the dry state (cf. Figure 5). As expected, the differential phase-contrast signal contains essentially horizontal components. It is evident that the dark-field signal has diagonal components not visible in the absorption and phase-contrast images.

By image analysis based on the absorption signal (cf. Figure 6), the water content in the sample has been estimated. As water increases the absorption, excess absorption compared to the dry case has been plotted with two shades of blue. Similar analysis can be based on the phase contrast and the dark field signal. It is clear from the results that one can track the drying process in the sample with this imaging technique. The moisture distribution resolving power, combined with the high penetration length of X-rays and the sensitivity of the dark-field signal to textile fabric details, suggests that grating interferometry can become a valuable tool for studying moisture transport, even in realistic multi-layered clothing systems. As imaging by grating interferometry in home-laboratories is based on a rather broad spectrum of X-ray photon energies, extracting quantitative information from these images is challenging, but would certainly be worth pursuing further, possibly with monochromatic X-ray radiation.[33]

Grating interferometry has essentially no depth sensitivity, but 3D images can be obtained by rotating the sample in the beam and applying reconstruction methods similar to those used in absorption-based computed

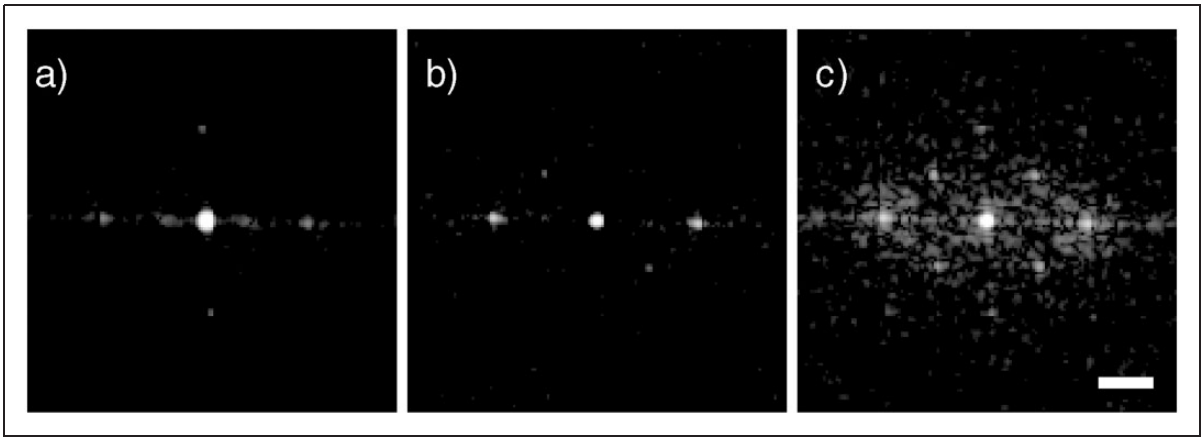

Figure 5. Fourier transform of (a) the absorption, (b) differential phase, and (c) dark-field contrast signals, all from the same dataset obtained on plain-weaved cotton fabric in the dry state. The intensity scaling is chosen for best visualization in each image individually. Scale bar is 10 mm^{-1}.

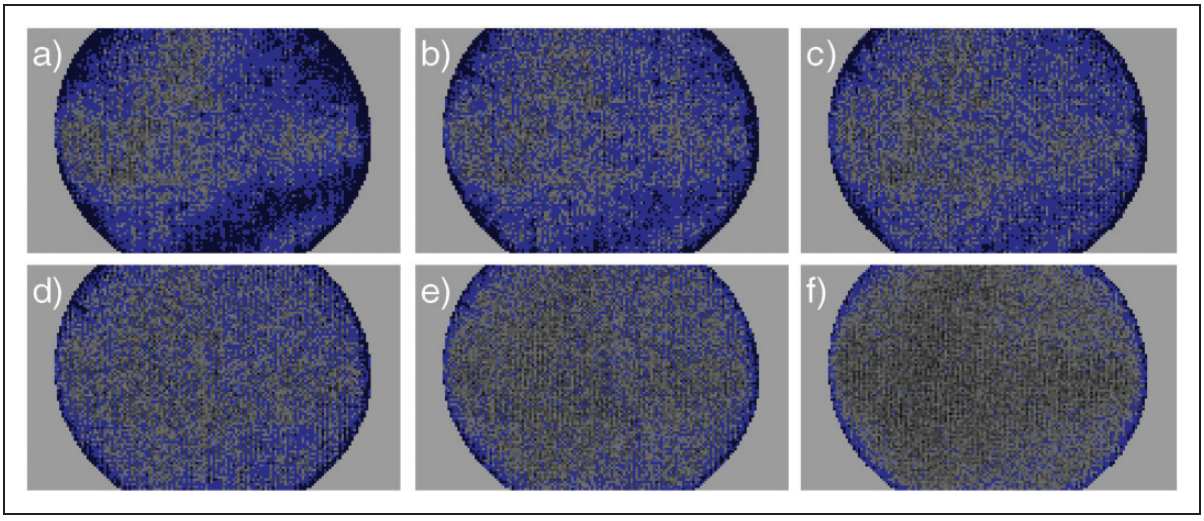

Figure 6. False-color interpretation based on the absorption-contrast images; the blue-colored regions have a substantial amount of water residing in the cotton. The images show a soaked sample in gradually drying up, starting from (a). The time interval between the images is about 5 minutes, and the diameter of the circular field of view is 25 mm.

tomography. We also note that the inherent directional sensitivity of the differential phase contrast signal can be used to distinguish different parts of the sample.[39,44] For multilayer textile samples, an effective depth-sensitivity can be obtained by differentiating the individual layers, e.g. based on differences in the textile weave pattern.

In summary, X-ray grating interferometry-based imaging resolves micron to millimeter sized features in the woven cotton, thus resolving individual yarns or fibers, but is also highly sensitive to textile wetting. Importantly for applied studies, the field of view is sufficiently large to study macroscopic samples.

Future outlook

While X-ray scattering, diffraction and radiography have been used for decades in a wide range of scientific fields, the new techniques discussed here are still largely in the development stage. Ptychography holds promise of a resolution in theory limited only by the maximum angle at which intensity scattered by the specimen can be reliably measured. It thus seems destined to become a complementary tool to electron microscopies, able to operate under in situ conditions, as demonstrated also in the present work. Samples of thicknesses of several tens of microns can easily be studied with

ptychography, which is thick compared to the <100 nm thickness usually required for transmission electron microscopy. Environmental scanning electron microscopy (ESEM) is a technique of growing importance,[11] but cannot be used to study the interior of samples like the wool fibers examined here without sectioning. Similarly, imaging by grating interferometry is developing rapidly as a characterization tool with large societal impact, having prospective applications in many fields also outside of academia. Grating interferometry is applicable to textiles in general, and the contrast seen here should be similar also for fabrics other than cotton.

While 3D imaging through computed tomography requires a time-consuming collection of many projections for both ptychography and grating interferometry, 2D images can be obtained using on the order of a minute per image with the current samples and setups. For ptychography, it is expected that near-future improvements will reduce the data collection time by at least one order of magnitude, which will facilitate time resolved measurements of ~1 second temporal resolution.

Describing both ptychography and grating interferometry in the same article, it is natural to point out some of their similarities and differences. They are both based on coherent X-ray radiation, and represent sophisticated methods that are gradually becoming available also to fields other than X-ray physics. Hard X-ray ptychography is a high resolution microscopy technique, and will, at least with today's known technology, have to be carried out at specialized synchrotron beamlines. Conversely, grating interferometry, while also fruitful with synchrotron sources,[45] arguably has as its main strength the fact that it is based on conventional X-ray sources. In both cases, we note that in future setups, simultaneously measuring the sample mass would be useful for extracting more quantitatively the wetting of the textile.

The possibility of measuring water transport in textile multilayers has been mentioned. Another natural extension of the current work would be to investigate 'smart' textile materials like Gore-Tex® membranes in a humidity gradient, for which the ptychography technique should allow the distribution of water partially wetting and permeating the membrane to be imaged. Similarly, comparative imaging studies of e.g., goose vs. eider down in humid conditions would be an interesting continuation of ideas presented here.

Conclusions

We have presented two original contributions on the applicability of in situ X-ray imaging for monitoring humidity in textile wool fibers and cotton woven fabrics. In situ X-ray ptychographic tomography performed on a single wool fiber at high and low humidity conditions with a 3D resolution of approximately 200 nm shows that wool fibers swell radially by 8–9% isotropically in the plane perpendicular to the main axis of the fiber. Quantitative information relating to the physical properties of the wool fiber like local electron density and mass density has been retrieved, and found to corroborate results reported for other experimental techniques, emphasizing the power of this non-destructive technique for in situ measurements. We also report results from grating interferometric imaging of a drying piece of woven cotton fabric. The field of view being in the range of centimeters combined with resolution in the micrometer range renders this technique highly suitable for textile studies. It is clear from the results that one can follow the drying process in the sample with this imaging technique. For the dry sample, the dark-field contrast gives the image that best resolves the many micron-sized details in the sample. The dark-field contrast is also found to be particularly sensitive to the presence of water. For the wet sample the phase image remains sensitive to the features of the textile, yielding good resolution and contrast. The sensitivity of the grating interferometry technique suggests a potential application of this technique for in situ studies of diffusive transport in two or three dimensions in organic samples in general, with a resolution approaching the micrometer range. We conclude that coherent imaging and microscopy techniques from the forefront of X-ray physics are on the verge of becoming highly useful tools for in situ studies of textile materials.

Funding

This work was supported by The Research Council of Norway (via the ColdWear project) and the industrial partners Statoil ASA, Total E&P Norge AS, Janus Holdings AS, Weenaas AS and Swix Sport AS, The Danish Council for Independent Research (via DANSCATT), the DFG Cluster of Excellence Munich-Centre for Advanced Photonics (MAP), the DFG Gottfried Wilhelm Leibniz program, and the European Research Council (ERC, FP7, StG 240142).

Acknowledgements

The authors wish to thank Ole Tore Buset for technical support. This work was carried out with support of the Karlsruhe Nano Micro Facility (KNMF, www.kit.edu/knmf), a Helmholtz Research Infrastructure at Karlsruhe Institute of Technology (KIT).

References

1. Anand S, Kennedy JF, Miraftab M and Rajendran S. *Medical and healthcare textiles*. Woodhead Publishing, 2010.

2. O'Mahony M. *Advanced textiles for health and well-being*. Thames & Hudson, 2011.
3. Mondal S. Phase change materials for smart textiles – an overview. *Appl Thermal Eng* 2008; 28: 1536–1550.
4. Saville BP. Physical testing of textiles. *Physical testing of textiles*. Woodhead Publishing, 1999.
5. Ahumada O, Cocca A, Gentile G, Martuscelli E and D'Orazio L. Uniaxial tensile properties of yarns: effects of moisture level on the shape of stress-strain curves. *Text Res J* 2004; 74: 1001–1006.
6. Esmaeili M, Fløystad JB, Diaz A, et al. Ptychographic X-ray tomography of silk fiber hydration. *Macromolecules* 2013; 46: 434–439.
7. Johnson NAG and Russell IM. *Advances in wool technology*. Taylor & Francis Group, 2008.
8. Hearle JWS. *Physical properties of wool*. The Textile Institute, Woodhead Publishing Limited, 2002.
9. Gordon S and Hsieh YL. *Cotton: Science and technology*. Woodhead, 2007.
10. Philip W, Noelie B, Alfred F, et al. Cotton fibers. *Handbook of fiber chemistry, Third Edition*. CRC Press, 2006.
11. Danilatos GD. *Foundations of environmental scanning electron microscopy*. Academic Press, 1988.
12. Nishiyama Y, Langan P and Chanzy H. Crystal structure and hydrogen-bonding system in cellulose 1 beta from synchrotron X-ray and neutron fiber diffraction. *J Am Chem Soc* 2002; 124: 9074–9082.
13. Feldkamp JM, Schroer CG, Patommel J, et al. Compact x-ray microtomography system for element mapping and absorption imaging. *Rev Sci Instrum* 2007; 78: 8.
14. Abbey B. From grain boundaries to single defects: a review of coherent methods for materials imaging in the X-ray sciences. *Jom* 2013; 65: 1183–1201.
15. Schroer CG, Kurapova O, Patommel J, et al. Hard x-ray nanoprobe based on refractive x-ray lenses. *Appl Phys Lett* 2005; 87: 124103-3.
16. Snigirev A, Snigireva I, Kohn V, Kuznetsov S and Schelokov I. On the possibilities of x-ray phase contrast microimaging by coherent high-energy synchrotron radiation. *Rev Sci Instrum* 1995; 66: 5486–5492.
17. Fienup JR. Phase retrieval algorithms: a comparison. *Appl Opt* 1982; 21: 2758–2769.
18. Pfeiffer F, Bech M, Bunk O, et al. X-ray dark-field and phase-contrast imaging using a grating interferometer. *J Appl Phys* 2009; 105: 102006-4.
19. Faulkner HML and Rodenburg JM. Movable aperture lensless transmission microscopy: a novel phase retrieval algorithm. *Phys Rev Lett* 2004; 93: 023903.
20. Rodenburg JM, Hurst AC, Cullis AG, et al. Hard-x-ray lensless imaging of extended objects. *Phys Rev Lett* 2007; 98: 034801.
21. Bunk O, Dierolf M, Kynde S, Johnson I, Marti O and Pfeiffer F. Influence of the overlap parameter on the convergence of the ptychographical iterative engine. *Ultramicroscopy* 2008; 108: 481–487.
22. Thibault P, Dierolf M, Bunk O, Menzel A and Pfeiffer F. Probe retrieval in ptychographic coherent diffractive imaging. *Ultramicroscopy* 2009; 109: 338–343.
23. Thibault P, Dierolf M, Menzel A, Bunk O, David C and Pfeiffer F. High-resolution scanning x-ray diffraction microscopy. *Science* 2008; 321: 379–382.
24. Maiden AM and Rodenburg JM. An improved ptychographical phase retrieval algorithm for diffractive imaging. *Ultramicroscopy* 2009; 109: 1256–1262.
25. Takahashi Y, Suzuki A, Zettsu N, et al. Towards high-resolution ptychographic x-ray diffraction microscopy. *Phys Rev B* 2011; 83: 5.
26. Vila-Comamala J, Diaz A, Guizar-Sicairos M, et al. Characterization of high-resolution diffractive X-ray optics by ptychographic coherent diffractive imaging. *Opt Express* 2011; 19: 21333–21344.
27. Dierolf M, Menzel A, Thibault P, et al. Ptychographic X-ray computed tomography at the nanoscale. *Nature* 2010; 467: 436–439.
28. Diaz A, Trtik P, Guizar-Sicairos M, Menzel A, Thibault P and Bunk O. Quantitative x-ray phase nanotomography. *Phys Rev B* 2012; 85: 020104.
29. Jacobsen C, Kirz J and Williams S. Resolution in soft X-ray microscopes. *Ultramicroscopy* 1992; 47: 55–79.
30. Holler M, Raabe J, Diaz A, et al. An instrument for 3D x-ray nano-imaging. *Rev Sci Instrum* 2012; 83: 073703–073707.
31. Pfeiffer F, Bech M, Bunk O, et al. Hard-X-ray dark-field imaging using a grating interferometer. *Nat Mater* 2008; 7: 134–137.
32. Momose A, Kawamoto S, Koyama I, Hamaishi Y, Takai K and Suzuki Y. Demonstration of X-Ray Talbot interferometry. *Jpn J Appl Phys Part 2* 2003; 42: L866–L868.
33. Bech M, Bunk O, Donath T, Feidenhans'l R, David C and Pfeiffer F. Quantitative x-ray dark-field computed tomography. *Phys Med Biol* 2010; 55: 5529.
34. Weitkamp T, Diaz A, David C, et al. X-ray phase imaging with a grating interferometer. *Opt Express* 2005; 13: 6296–6304.
35. Tapfer A, Bech M, Velroyen A, et al. Experimental results from a preclinical X-ray phase-contrast CT scanner. *PNAS* 2012; 109: 15691–15696.
36. Pfeiffer F, Weitkamp T, Bunk O and David C. Phase retrieval and differential phase-contrast imaging with low-brilliance X-ray sources. *Nat Phys* 2006; 2: 258–261.
37. Talbot HF. LXXVI. Facts relating to optical science. No. IV. *Phil Mag Ser 3* 1836; 9: 401–407.
38. Berry M, Marzoli I and Schleich W. Quantum carpets, carpets of light. *Phys World* 2001; 14: 39–44.
39. Jensen TH, Bech M, Bunk O, et al. Directional x-ray dark-field imaging. *Phys Med Biol* 2010; 55: 3317.
40. Kraft P, Bergamaschi A, Bronnimann C, et al. Characterization and calibration of Pilatus detectors. *IEEE Trans Nucl Sci* 2009; 56: 758–764.
41. Guizar-Sicairos M, Diaz A, Holler M, et al. Phase tomography from x-ray coherent diffractive imaging projections. *Opt Express* 2011; 19: 21345–21357.

42. Bech M. X-ray imaging with a grating interferometer. *PhD thesis*. Denmark: University of Copenhagen, 2009.
43. Hearle JWS. *High-performance fibres*. Textile Institute, 2001.
44. Zanette I, Weitkamp T, Donath T, Rutishauser S and David C. Two-dimensional X-ray grating interferometer. *Phys Rev Lett* 2010; 105.
45. Weitkamp T, Zanette I, David C, et al. Recent developments in X-ray Talbot interferometry at ESRF-ID19. In: Stock SR (ed.) *Developments in X-Ray Tomography Vii*. 2010.